Available online at www.sciencedirect.com

ScienceDirect

Scripta Materialia 103 (2015) 69–72

Scripta MATERIALIA

www.elsevier.com/locate/scriptamat

Time-resolved synchrotron tomographic quantification of deformation-induced flow in a semi-solid equiaxed dendritic Al–Cu alloy

B. Cai,[a,b] S. Karagadde,[a,b] D. Rowley,[a,b] T.J. Marrow,[c] T. Connolley[d] and P.D. Lee[a,b,*]

[a]*School of Materials, University of Manchester, Manchester, UK*
[b]*Research Complex at Harwell, Rutherford Appleton Laboratory, Harwell, Oxfordshire, UK*
[c]*Department of Materials, University of Oxford, Oxford, UK*
[d]*Diamond Light Source Ltd., Harwell Science and Innovation Campus, Didcot, UK*

Received 13 November 2014; revised 2 March 2015; accepted 3 March 2015
Available online 27 March 2015

The rheology of semi-solid alloys has been studied by a novel *in situ* tomographic technique. Via extruding an equiaxed Al–15 wt.%Cu alloy, the inhomogeneous coherent compression of the α-Al grains was quantified, including the interdendritic channel closure and formation of a liquid extrudate. This investigation not only provides important insights into the microstructural changes occurring during semi-solid deformation, but also offers a validation benchmark for segregation and rheological models.

Keywords: Semi-solid deformation; Segregation; Liquid flow; X-ray tomography

Understanding liquid migration through a deforming semi-solid medium is critical for a wide range of processes from metal casting [1,2] to volcanology [3–5]: during casting, deformation of semi-solid alloys can influence liquid flow, resulting in macrosegregation, which can degrade the mechanical properties of the final product [2,6–10]; semi-solid magma is deformed by convection and/or tectonic plate spreading, inducing melt migration and segregation [3,4,11].

In solidification processing, deformation in the semi-solid can induce a range of defects, including extrusion segregation in squeeze-casting [1] and surface exudation in direct-chill casting [7]. Although several prior investigations have identified deformation-driven melt flow as a possible mechanism of such defects [1,7,12], the influence of stress on a semi-solid alloy and the melt flow through the equiaxed microstructure are not clearly understood. Many models have been developed to predict the formation of those defects, based on the proposition of the mushy zone as a sponge saturated with liquid [2,7,13,14]. However, currently there are no direct validation techniques that capture the kinetics incorporated in this hypothesis; *in situ* synchrotron tomography is one possible solution.

Recently, high speed X-ray tomography has been utilized to perform four dimensional imaging (4D, i.e. 3D plus time) of the pore-scale fluid flow [15], solidification [16–18], and the influence of deformation on semi-sold alloys [19–21]. Tensile and uniaxial compression tests have been used previously with the help of 4D imaging to study semi-solid deformation; these were mainly focused on the formation of damage (hot tearing) as a result of the granular response of the mushy zone [19,21,22]. In this paper, we describe the application of an indirect extrusion cell to study the rheological behavior of the mushy zone and the mechanisms responsible for the liquid migration induced by deformation. Such an indirect extrusion cell can also be used to study how extrusion segregation and exudation form, since it mimics their forming conditions.

The sample was semi-solid, equiaxed dendritic Al–15 wt.%Cu; a cylindrical specimen 2.9 mm in diameter by 2.9 mm long was prepared using wire electro-discharge machining, and then inserted in a boron nitride holder with an inner diameter (ID) of 3 mm and outer diameter (OD) of 5 mm. An alumina tube (1.5 mm ID and 3 mm OD) was placed on top of the specimen forming an indirect extrusion cell (Fig. 1). The entire extrusion set-up was enclosed within a resistive furnace [21], mounted on a bespoke mechanical testing rig with inbuilt rotation (P2R [20,21]).

The experiment was conducted using 53 keV monochromatic X-rays on the I12 beamline at Diamond Light Source. A high speed X-ray imaging system was used,

* Corresponding author at: School of Materials, University of Manchester, Manchester, UK.

http://dx.doi.org/10.1016/j.scriptamat.2015.03.011
1359-6462/

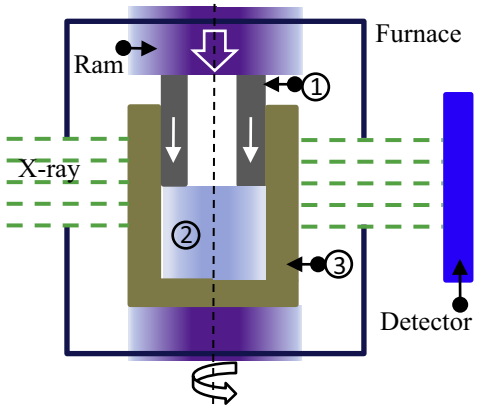

Figure 1. Schematic of the extrusion cell and *in situ* resistance furnace: 1 – alumina tube; 2 – specimen; 3 – boron nitride holder.

consisting of the beamline's custom-built imaging modules coupled to a CMOS camera (Miro 310M, Vision Research, USA). The imaging system provided a field of view (FOV) of 5.12 × 3.2 mm and 4 μm pixel size. The sample was positioned so that the top half of the billet and extrudate was in the FOV. The sample was heated to 560 ± 2 °C (27 ± 3% liquid fraction) in 15 min, and then held for 10 min for thermal homogenization. Subsequently, the top ram was moved down at 1 μm/s, forcing the alumina tube downwards while measuring loads.

Seven tomograms were captured, each comprising 900 radiographs, collected within 9 s at 45 s intervals. A filtered back projection algorithm was used to reconstruct the data to generate a tomography (unsigned 16-bit integral) [23]. Noise reduction was performed using a 3D median filter, followed by an anisotropic diffusion filter [24] using Avizo 8 (FEI VSG, France). Liquid phases were segmented by the Otsu method [25] using MATLAB 2012b (The Mathworks Inc., USA); errors were evaluated by varying the threshold value (24108) by ±50.

Figure 2a–c displays the resulting 2D longitudinal slices of the specimen under extrusion at the displacements of 0, 162 and 324 μm, respectively. The dark gray dendrites are the α-Al grains, while the Cu-enriched liquid is light gray. The corresponding 3D volume-rendered image is shown in the Supplementary information. A small amount of liquid segregated into the tube on top of the sample is notable (Fig. 2a at $d = 0$ μm); this extrudate is due to the stress caused by thermal expansion during heating. The subsequent response of the mush to the applied deformation is shown in Fig. 2b (162 μm) and Fig. 2c (324 μm). As deformation progressed, more melt flowed into the alumina tube from the semi-solid specimen. The liquid channels under the wall of the extrusion tube closed in response to the deformation (zone D in Fig. 2b and c). The evolution of the extruded liquid (Fig. 2e–g) displayed the characteristic profile of laminar flow in a pipe. We can also observe the closure of pre-existing porosity (Fig. 2e–i) due to the compressive strain.

In addition to making the above qualitative observations, we performed a detailed, time-resolved quantification of the extrusion. From $d = 0$ to 324 μm, the volume of the expelled liquid in the tube increased from ≈0.2 to ≈2 mm^3 at an almost constant rate of ≈0.0055 mm^3 per μm displacement. The extruded liquid volume increased at the same rate as the volumetric displacement (≈0.0053 $mm^3/\mu m$) of the alumina tube. The liquid fraction in the billet (lower part of the specimen) decreased from 26.7 ± 2.8% to 15.1 ± 2.1%, indicating densification of the mush (Fig. 3b). The extraction of the liquid by compression of the solid skeleton can be understood by considering the mush to be a saturated sponge, consisting of two phases (the solid grains and the liquid phase). This observation is contrary to the shear-induced dilation that is observed during direct shearing [26] and uniaxial semi-solid compression of equiaxed dendrites [21] and globular grains [22], where the liquid channels locally open rather than close. This suggests that different stress states can alter the fluid flow via different mechanisms (sponge or granular). The experiment reveals that constrained compressive stress densifies the solid skeleton and expels liquid from the mush (spongy-like behavior); shear stress is known to cause dilation, drawing liquid from the surrounding neighborhood into the dilated spaces between the grains (granular behavior) [21]. Therefore, when modeling semi-solid deformation, the effect of the stress states on the modulation of liquid flow needs be accounted for.

Along with liquid, a small amount of the solid phase was ejected into the die cavity (Fig. 2d–f). The peak height of extruded solid increased gradually (Fig. 3a). A magnified view of the extruded grains is shown in Figure 2j and k. Those grains located near the extruder inlet were free to move and appear to be sheared by the grains below, leading to dilatant translation and rotation (e.g. the grain A moved

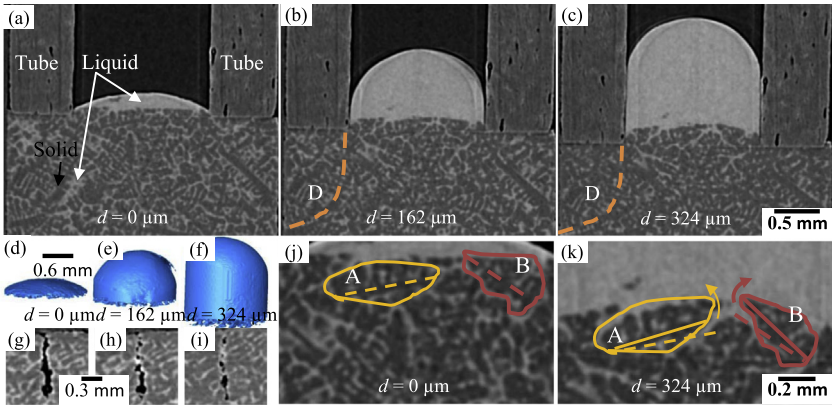

Figure 2. (a–c) 2D longitude slices of Al15Cu extruded at increasing vertical displacement; (d–f) 3D profile of the extrudate; (g–i) pore closure during extrusion; (j and k) magnified view showing the grain movements near the extruder inlet.

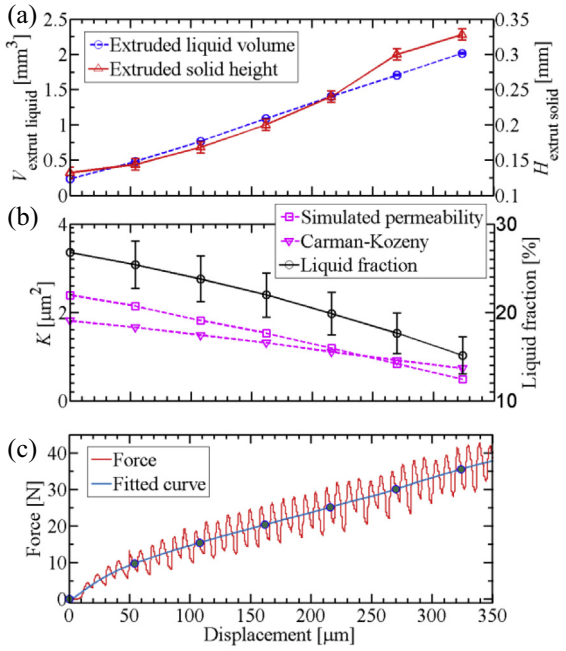

Figure 3. (a) Liquid volume and solid being squeezed out during semi-solid extrusion; (b) liquid fraction, permeability calculated from Navier–Strokes equation and Carman–Kozeny relationship; (c) the force versus displacement (the periodicity fluctuation of force is due to sample rotation).

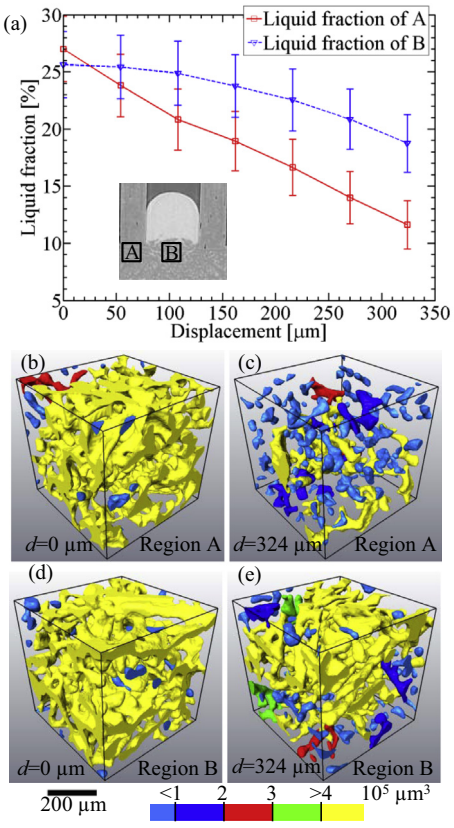

Figure 4. (a) Liquid volume fraction in Region A and B (see insert) vs. displacement; (b–e) 3D view of liquid channels and droplets colored according their volume in Region A and B.

down ≈0.3 mm and rotated ≈7° in anticlockwise direction, while grain B underwent ≈12° clockwise rotation). Consequently, the liquid-filled interstitial space increased slightly (Fig. 2k). Buoyancy forces might also play a role in the grain movement as the Cu-rich liquid is denser than the α-Al solid. The movement of grains due to deformation and associated changes of interdendritic liquid will cause both compositional and microstructural variation in the final component.

Determining the mechanical response of the mush requires knowledge of the strength of the dendritic/globular α-Al network and the resistance of the liquid flow. Although calculating the strength of α-Al network would require complex simulations, we can use the 3D geometry of the liquid network to directly determine the permeability, or resistance to the flow of the interdendritic liquid. This was done by solving the Navier–Strokes equations on a subset of the mush at each time step. A subvolume of $2 \times 2 \times 0.8$ mm was extracted from the central region of the sample within the billet. Avizo XLab flow simulation code (FEI VSG, France) was used for the simulations (conditions detailed in Ref. [16]). The simulation is also compared with the Carman–Kozeny permeability relationship [27]:

$$K = \frac{f_l^3}{k_c S_V^2} \tag{1}$$

where f_l is the liquid fraction, S_V is the surface area of the solid per unit volume of sample measured directly from the 3D data, and k_c (the Kozeny constant) is set to 5 as suggested by Duncan et al. [28]. The simulated permeability decreased monotonically from ≈2.4 to ≈0.5 μm^2 during the 324 μm of extrusion (Fig. 3b). Although there is disparity between the simulation and Carman–Kozeny equation, this is still within the scatter of previous work [29]. The continuous decrease of permeability shows the extrusion continued to compress the solid skeleton, increasing the flow resistance and blocking further flow of the interdendritic liquid.

The force measurement (Fig. 3c) provides additional information on the mechanical response of the semi-solid specimen. The load linearly rose from 9.7 ± 1.6 N at $d = 54$ μm, to 35.5 ± 2.5 N at 324 μm. The load increase rate is roughly linear at 0.1 N/μm. It is likely that further densification of the mush will significantly increase the stress as observed by Ludwig et al. [30]. Note that although the measured force is a combined response of liquid flow and solid deformation resistance of the mush, it is expected the liquid flow resistance is minimal as compared to the mechanical load of α-Al network. Figure 3a–c established the correlation of the rheological properties with the evolving two phase microstructure.

Although the measured bulk properties (force, liquid fraction, permeability and expelled liquid volume) are linear with time, the deformation is inhomogeneous. This has been quantified by determining the liquid fraction within different regions (A and B in Figure 4a insert) in the billet. Figure 4a reveals that the liquid fraction of Region A decreased faster than that of B. At the initial stage of deformation ($d = 0$ μm, Fig. 4b and d), the liquid flowed through a complex network, which was homogeneously distributed and well connected with few isolated liquid pockets. During the extrusion, a considerable rise in the number density of

isolated liquid pockets was observed from ≈224 to ≈896 mm^{-3} in Region A, while Region B showed a marginal increase (≈320 to ≈448 mm^{-3}). At the final stage, more liquid pockets were observed in Region B than in A at 324 μm (Fig. 4c and e). Compressive deformation narrowed the liquid channels and closed them at their throats. The inhomogeneous nature of deformation is due to the fact that the propagation of compression in granular medium is strongly dependent on the microstructure and tends to follow the percolating pathways [31].

In conclusion, a novel technique combining high speed synchrotron X-ray tomography and mechanical deformation was developed to measure the influence of microstructure on the rheological behavior of semi-solids. The potential of the technique has been demonstrated by observing and quantifying the rheology of a semi-solid equiaxed dendritic Al–15 wt.%Cu alloy. The real time 3D quantification of semi-solid extrusion provided new insights into the behavior of a mush, as follows: the strain distribution is very inhomogeneous due to the sponge-like compression of the partially coherent equiaxed dendritic solid; the strain is mostly accommodated by inter and intra-grain compaction, with only a small amount of granular flow; the interdendritic liquid is driven out of the semi-solid mush and forms an extrudate; and the permeability of the compacting mush approximately follows a Carman–Kozeny relationship. These microstructural level observations can be directly used to develop and validate segregation and rheological models.

This work was financially supported by the United Kingdom EPSRC (EP/I02249X/1) and the European Union (RFSR-PR-10005 DDT). We thank Diamond Light Source for beamtime visit (EE9018-1), and we are grateful to Vision Research UK for the loan of the Miro 310M. B.C. acknowledges General Electric and China Scholarship Council for funding his PhD.

Supplementary data associated with this article can be found, in the online version, at http://dx.doi.org/10.1016/j.scriptamat.2015.03.011.

[1] T. Rølland, R. Flatval, L. Arnberg, Mater. Sci. Eng. A 173 (1993) 267.
[2] J. Dantzig, M. Rappaz, Solidification: Methods, Microstructure and Modeling, EFPL Press, 2009.
[3] R.F. Katz, M. Spiegelman, B. Holtzman, Nature 442 (2006) 676.
[4] J.E. Kendrick, Y. Lavallée, T. Hirose, G. Di Toro, A.J. Hornby, S. De Angelis, D.B. Dingwell, Nat. Geosci. 7 (2014) 438.
[5] Y. Lavallée, P.G. Meredith, D.B. Dingwell, K.-U. Hess, J. Wassermann, B. Cordonnier, A. Gerik, J.H. Kruhl, Nature 453 (2008) 507.
[6] P.D. Lee, P.E. Ramirez-Lopez, K.C. Mills, B. Santillana, Ironmak. Steelmak. 39 (2012) 244.
[7] H. Thevik, A. Mo, T. Rusten, Metall. Mater. Trans. B 30 (1999) 135.
[8] D.G. Eskin, Physical Metallurgy of Direct Chill Casting of Aluminum Alloys, CRC Press, 2008.
[9] R. Nadella, D.G. Eskin, Q. Du, L. Katgerman, Prog. Mater. Sci. 53 (2008) 421.
[10] C. Beckermann, Int. Mater. Rev. 47 (2002) 243.
[11] B.K. Holtzman, D.L. Kohlstedt, M.E. Zimmerman, F. Heidelbach, T. Hiraga, J. Hustoft, Science 301 (2003) 1227.
[12] H. Shen, C. Beckermann, Metall. Mater. Trans. B 33 (2002).
[13] G. Lesoult, C.A. Gandin, N.T. Niane, Acta Mater. 51 (2003) 5263.
[14] L. Nicolli, A. Mo, M. M'Hamdi, Metall. Mater. Trans. A 36 (2005) 433.
[15] S. Berg, H. Ott, S.A. Klapp, A. Schwing, R. Neiteler, N. Brussee, A. Makurat, L. Leu, F. Enzmann, J.-O. Schwarz, M. Kersten, S. Irvine, M. Stampanoni, Proc. Natl. Acad. Sci. U.S.A. 110 (2013) 3755.
[16] C. Puncreobutr, A.B. Phillion, J.L. Fife, P.D. Lee, Acta Mater. 64 (2014) 316.
[17] O. Ludwig, M. Dimichiel, L.U.C. Salvo, M. Suéry, P. Falus, Metall. Mater. Trans. A 36 (2005) 1515.
[18] L.K. Aagesen, J.L. Fife, E.M. Lauridsen, P.W. Voorhees, Scr. Mater. 64 (2011) 394.
[19] S. Terzi, L. Salvo, M. Suéry, N. Limodin, J. Adrien, E. Maire, Y. Pannier, M. Bornert, D. Bernard, M. Felberbaum, Scr. Mater. 61 (2009) 449.
[20] C. Puncreobutr, P.D. Lee, R.W. Hamilton, B. Cai, T. Connolley, Metall. Mater. Trans. A 44 (2012) 5389.
[21] B. Cai, S. Karagadde, L. Yuan, T.J. Marrow, T. Connolley, P.D. Lee, Acta Mater. 76 (2014) 371.
[22] K.M. Kareh, P.D. Lee, R.C. Atwood, T. Connolley, C.M. Gourlay, Nat. Commun. 5 (2014) 4464.
[23] S. Titarenko, P.J. Withers, A. Yagola, Appl. Math. Lett. 23 (2010) 1489.
[24] D. Bernard, O. Guillon, N. Combaret, E. Plougonven, Acta Mater. 59 (2011) 6228.
[25] N. Otsu, Syst. Man Cybern. IEEE Trans. 9 (1979) 62.
[26] T. Nagira, S. Morita, H. Yokota, H. Yasuda, C.M. Gourlay, M. Yoshiya, A. Sugiyama, K. Uesugi, A. Takeuchi, Y. Suzuki, Metall. Mater. Trans. A 45 (2014) 5613.
[27] P.C. Carman, Flow of Gases through Porous Media, Butterworths, London, 1956.
[28] A.J. Duncan, Q. Han, S. Viswanathan, Metall. Mater. Trans. B 30 (1999) 745.
[29] D. Bernard, O. Nielsen, L. Salvo, P. Cloetens, Mater. Sci. Eng. A 392 (2005) 112.
[30] O. Ludwig, J. Drezet, C.L. Martin, M. Suéry, Metall. Mater. Trans. A 36 (2005) 1525.
[31] R. Pastor-Satorras, M.-C. Miguel, J. Stat. Mech. Theory Exp. 2012 (2012) P02008.